IOP PUBLISHING PLASMA PHYSICS AND CONTROLLED FUSION

Plasma Phys. Control. Fusion **51** (2009) 024011 (13pp) doi:10.1088/0741-3335/51/2/024011

All-optical control of nonlinear focusing of laser beams in plasma beat wave accelerator

Serguei Kalmykov, S Austin Yi and Gennady Shvets

Department of Physics and Institute for Fusion Studies, The University of Texas at Austin, One University Station C1500, Austin, Texas 78712, USA

E-mail: kalmykov@physics.utexas.edu

Received 10 May 2008, in final form 25 August 2008
Published 7 January 2009
Online at stacks.iop.org/PPCF/51/024011

Abstract

Nonlinear focusing of a bi-color laser in plasma can be controlled by varying the difference frequency Ω. The driven electron density perturbation forms a co-moving periodic focusing (de-focusing) channel if Ω is below (above) the electron Langmuir frequency ω_p. Hence, the beam focusing is enhanced for $\Omega < \omega_p$ and is suppressed otherwise. In particular, a catastrophic relativistic self-focusing of a high-power laser beam can be prevented all-optically by a second, much weaker, co-propagating beam shifted in frequency by $\Omega > \omega_p$. A bi-envelope equation describing the early stage of the mutual de-focusing is derived and analyzed. Later stages, characterized by a well-developed electromagnetic cascade, are investigated numerically. Stable propagation of the over-critical laser pulse over several Rayleigh lengths is predicted. The non-resonant plasma beat wave ($\Omega \neq \omega_p$) can accelerate pre-injected electrons above 100 MeV with low energy spread.

(Some figures in this article are in colour only in the electronic version)

1. Introduction

Electron acceleration in the plasma waves driven by high-intensity lasers [1] has been an important research topic in the advanced accelerator community over the last two decades [2, 3]. Accelerating gradient in the near-luminous plasma wave can exceed 1 GeV m^{-1}, which opens the way to table-top accelerators. Prospective applications [4], however, require not only high gradient but also shot-to-shot stability and high quality of accelerated bunches. The latter can be impaired by the nonlinear processes such as relativistic self-focusing (RSF) of the laser beam [5–7]. The phenomenon of self-focusing occurs due to the nonlinear dependence of refractive index on the laser intensity, and is universal to a variety of media: from solid optical fibers to gaseous plasmas [8]. In plasmas, the index variation can be caused by the relativistic mass increase of an electron oscillating in the laser field [5–7, 9–11]. If the

peak laser power exceeds the threshold $P_{cr} = 16.2(\omega_0/\omega_p)^2$ GW [7] (where ω_0 is the laser frequency, $\omega_p = (4\pi e^2 n_0/m_e)^{1/2} \ll \omega_0$ is the electron plasma frequency, n_0, $-e$ and m_e are, respectively, the electron background density, charge and rest mass), the RSF overcomes diffraction, and the beam collapses. Electron cavitation [7, 9] or higher-order relativistic nonlinearities [10, 11] saturate the RSF. When a long ($\tau_L \gg 1/\omega_p$) *bi-color* laser beam with a frequency difference Ω propagates in plasma (the situation typical of the plasma beat wave accelerator, PBWA [1]), the phenomenon of nonlinear focusing becomes multi-faceted. The relativistic cross-focusing (RCF) further enhances the focusing effect [12–14]. At the same time, the periodic ponderomotive force drives a three-dimensional (3D) electron plasma wave (EPW) which acts as an either focusing (if $\Omega \leqslant \omega_p$) or de-focusing (if $\Omega > \omega_p$) periodic channel [14–17]. Interplay between the relativistic mass effects and ponderomotive nonlinearity can either enhance or suppress the nonlinear focusing of the entire multi-beam system [14].

The fact that the EPW driven at $\Omega \leqslant \omega_p$ dramatically enhances the bi-color beam focusing had been recognized very early [18, 19]. It is now well understood that the optical mixing of two under-detuned lasers ($\Omega \leqslant \omega_p$) results in the feedback loop between the laser beam focusing and the plasma wave excitation [20, 21]. Hence, the system becomes extremely vulnerable to the 3D amplitude self-modulation (resonant modulational instability, RMI) [22–25]. Simulations presented in section 4.2 of this paper, as well as our earlier studies [26, 27], support this conclusion.

Conversely, *de-focusing* effect of the *over-detuned* EPW ($\Omega > \omega_p$) counteracts the RSF and RCF; under favorable conditions (specified for the first time in this paper), the balance between the relativistic and ponderomotive nonlinearities can stabilize the system and result in a dynamical guiding of multi-color laser beam over several Rayleigh lengths without a preformed plasma channel. The latter effect, unlike the earlier studied [28, 29] reduction of RSF for ultrashort pulses ($\tau_L < 1/\omega_p$), takes place for long beams with a large energy content. In this paper, we pay a special attention to the regime where the catastrophic RSF of an over-critical ($P > P_{cr}$) laser beam is prevented all-optically by a second, much weaker, co-propagating over-detuned beam. At the same time, the driven EPW has a multi-GV m^{-1} accelerating gradient, which opens the window for the PBWA without external optical guiding.

The paper is organized as follows. In section 2 we derive the 3D weakly nonlinear paraxial model for the propagation of multi-color laser beams in plasmas. The nonlinear index corrections are calculated in the approximation of *local* electron response (the Kerr-type nonlinearity). An index variation due to the relativistic electron mass increase is local for pulses longer than one optical cycle. Assumption of the local ponderomotive nonlinearity is more restrictive and requires (a) laser duration above $2\pi/|\Omega - \omega_p|$ and (b) total absence of the relativistic effects in the longitudinal electron motion [30]. As a consequence, different transverse cross-sections of the multi-color beam evolve independently in the course of propagation. The non-instantaneous phenomena such as the seeded RMI [20, 21] and near-forward stimulated forward Raman scattering (SRS) [21, 25] are thus excluded, but the electromagnetic cascading [14, 15, 30–32] persists.

In section 3 we concentrate on the nonlinear focusing of multi-color laser beams. Sections 3.1 and 3.2 examine the tendency of the bi-color laser to focus or de-focus after entering the plasma. Building upon the model of section 2 and using the source-dependent expansion (SDE) [33], we derive the coupled evolution equations for the individual spot sizes. Their stationary points give the nonlinear focusing thresholds (in terms of a frequency mismatch $\Omega - \omega_p$, power partition between the components, and the ratio of initial spot sizes). These general expressions explicitly include (and thus allow one to distinguish between) the contributions from the relativistic mass effect and the plasma wave focusing. The extra focusing (in addition to the relativistic focusing) provided by the EPW driven by an *under-detuned* laser

beat wave has been extensively studied in [14, 15] (see the corresponding figure 4 of [14]). However, focusing *suppression* provided by the EPW driven by an *over-detuned* laser beat wave (corresponding to $\delta < 0$, using the definition of [14]) is considered here for the first time. In section 3.3 we explore numerically the dynamically guided propagation of the over-critical multi-frequency laser beam with $\Omega > \omega_p$. Quasi-guided propagation (with the spot size and peak intensity slowly varying over three Rayleigh lengths) is observed in the fully dynamic, relativistic 3D (with axial symmetry) particle-in-cell (PIC) simulation by the code WAKE [9]. Calculations based on the quasi-stationary model of electromagnetic cascade from section 2 well agree with the WAKE simulation over the initial stage of propagation (about one Rayleigh length).

Section 4 discusses numerical experiments on acceleration of pre-injected test electrons. It has been proposed and experimentally verified earlier [34] that the non-resonant plasma beat wave ($\Omega \gg \omega_p$) can accelerate electrons quite effectively. Here we focus on the near-resonant regimes ($\Omega \approx \omega_p$). Un-phased particles from a long ($\tau_b > 1/\omega_p$) and slow (initial energy $\sim$7.5 MeV) electron bunch (typical of a modern radio-frequency (RF) gun [35]) are trapped and accelerated in the over-detuned plasma wave (accelerating gradient $\sim$4 GV m^{-1}). Quasi-monoenergetic electron bunches with the energy above 100 MeV are observed. On the other hand, the under-detuned plasma beat wave ($\Omega < \omega_p$) reveals much higher accelerating gradient (tens of GV m^{-1}) but much worse laser stability. The WAKE simulations reveal a feedback loop between the plasma wave-enforced focusing and the plasma wave excitation; in this case the system evolution follows the scenario of seeded self-modulation [20, 21]. Dynamical focusing of the laser is much stronger than that inferred from the quasi-stationary model; the plasma wave evolution stabilizes only after the laser beam breakup at a considerable distance from the plasma boundary. Because of the initial plasma wave evolution, the quasi-monoenergetic acceleration requires electron injection inside the plasma slab (possibly with one of the all-optical techniques [36]).

The results are summarized in conclusion.

2. Basic equations

In this section we describe the propagation of a multi-color laser beam (electromagnetic cascade) in plasmas in a 3D geometry with the local (Kerr-type) ponderomotive nonlinearity. Our theoretical model is applicable to long laser pulses and excludes the spontaneous SRS and RMI. The independent variables are $(\boldsymbol{r}_\perp, z, \xi)$, where $\boldsymbol{r}_\perp = (x, y)$ is the transverse radius vector, z is the distance along the axis (propagation variable), and $\xi = ct - z$. The normalized (to $m_e c^2/|e|$) vector potential of the arbitrarily polarized laser beam is $\boldsymbol{a}(\boldsymbol{r}_\perp, z, \xi) = \mathrm{Re}[\boldsymbol{e}_0 a(\boldsymbol{r}_\perp, z, \xi)]$, where $\boldsymbol{e}_0$ is the unit complex vector of polarization. We assume that the bi-color laser beam with a difference frequency $\Omega \ll \omega_0$ is focused onto the plasma boundary $z = 0$. The vector potential at the boundary is prescribed:

$$a(\boldsymbol{r}_\perp, 0, \xi) = \mathrm{e}^{-\mathrm{i}k_0\xi}[a_0(\boldsymbol{r}_\perp, 0, \xi) + a_1(\boldsymbol{r}_\perp, 0, \xi)\mathrm{e}^{-\mathrm{i}k_\Omega\xi}]. \tag{1}$$

Here $k_0 = \omega_0/c$, $k_\Omega = \Omega/c$. Ions form an immobile neutralizing background due to the short laser duration. A co-moving electron density grating is produced by the ponderomotive beat wave. The co-moving modulation of index, in turn, produces the cascade of laser sidebands,

$$a(\boldsymbol{r}_\perp, z > 0, \xi) = \sum_{l=-\infty}^{+\infty} a_l(\boldsymbol{r}_\perp, z, \xi)\mathrm{e}^{-\mathrm{i}k_l\xi}, \tag{2}$$

where l is an integer, $k_l = k_0 + lk_\Omega$. The amplitudes a_l vary slowly in ξ on the scale k_Ω^{-1}, and their evolution is determined by the nonlinear plasma response. We expand the

electron density perturbation in harmonics phase-locked with the driving ponderomotive force, $n_e(\boldsymbol{r}_\perp, z, \xi) - n_0 = \frac{1}{2}\sum_l \delta n_l(\boldsymbol{r}_\perp, z, \xi)\mathrm{e}^{\mathrm{i}lk_\Omega\xi}$, where $\delta n_{-l} = \delta n_l^*$, $|\delta n_l| \ll n_0$ and $|\partial\delta n_l/\partial\xi| \ll k_\Omega|\delta n_l|$. Equations of cold electron hydrodynamics express δn_l through the laser intensity moments $\rho_l = \sum_m a_m a_{m+l}^*$,

$$N_l(\boldsymbol{r}_\perp, z, \xi) \approx \frac{1}{2}\frac{(l\Omega)^2}{(l\Omega)^2 - \omega_\mathrm{p}^2}\rho_l(\boldsymbol{r}_\perp, z, \xi), \tag{3}$$

where $\omega_l = \omega_0 + l\Omega$, and $N_l = \delta n_l/n_0$. The approximation (3) is well justified for the non-resonant beat wave, $|\Omega - \omega_\mathrm{p}| \geqslant 3\omega_\mathrm{RL} \gg 1/\tau_\mathrm{L}$ [30], where $\omega_\mathrm{RL} = (1/4)(3|a_0a_1|^2/2)^{1/3}$ is the Rosenbluth-Liu saturation frequency [37]. This condition totally eliminates the relativistic mass effects associated with the longitudinal electron motion. Equation (3) also implies that the ponderomotive force is predominantly longitudinal (i.e. the laser spot exceeds $k_\mathrm{p}^{-1} = c/\omega_\mathrm{p}$). Plasma response in the form (3) excludes such dynamic effects as spontaneous near-forward SRS and RMI and is thus limited to the initial stage of laser propagation.

Starting from the Maxwell equations for the laser beams, using equation (3), and applying a weakly relativistic approximation (i.e. calculating plasma currents with the accuracy $\sim \mathrm{O}(a^3)$), we obtain a set of coupled nonlinear paraxial envelope equations,

$$(2\mathrm{i}k_l\partial/\partial z + \Delta_\perp)a_l = k_l^2(1 - \eta_l^2)a_l, \tag{4}$$

where $\Delta_\perp = \partial^2/\partial x^2 + \partial^2/\partial y^2$, and η_l is the nonlinear index,

$$\eta_l^2 = 1 - (k_\mathrm{p}^2/k_l)^2[(l\Omega/\omega_0)^2 + (1/2)\sum_m (a_{m+l}/a_l)(N_m - \rho_m/2)]. \tag{5}$$

The first term in square brackets represents the group velocity dispersion (GVD) of radiation in plasmas. The second is the contribution from nonlinearities, i.e. the driven electron density perturbations (3) and the relativistic mass increase of an electron oscillating in the transverse fields. Under the assumptions from the previous paragraph, contribution from the relativistic mass effects in the longitudinal motion is of the higher order than $\mathrm{O}(a^3)$, and is thus neglected. This simplification is adequate for the calculation of the plasma wave-induced focusing [14]. On the other hand, equation (5) incorporates the (missing in the earlier 3D cascade model [14]) contributions from the ponderomotive force harmonics and the GVD. These terms are important for the long-term dynamics of the fully developed cascade [30, 32].

In the remainder of the paper we consider the co-axial propagation of axi-symmetric beams; hence, $\Delta_\perp \equiv r^{-1}\partial/\partial r + \partial^2/\partial r^2$, where $r = (x^2 + y^2)^{1/2}$. In the finite system ($1 \leqslant M < \infty$) of interacting beams the action $I = \int_0^\infty \sum_l k_l|a_l|^2 r\,\mathrm{d}r$ is conserved. Multiplying (4) by a_l^*, subtracting the complex conjugate, and summing up over l gives the identity $\sum_l k_l\partial|a_l|^2/\partial z = \mathrm{Im}\sum_l a_l\Delta_\perp a_l^*$, which, upon integration over r, gives the conservation of action (or Manley–Rowe relation): $\partial I/\partial z = 0$. Evolution of the entire multi-frequency beam (2) can be characterized in terms of the mean-square (action weighted) radius $\langle r^2\rangle \equiv I^{-1}\int_0^\infty r^2\sum_l k_l|a_l|^2 r\,\mathrm{d}r$ [14]. The beam focuses if $\partial\langle r^2\rangle/\partial z < 0$ and de-focuses otherwise. We start the next section with the derivation of the nonlinear focusing thresholds.

3. Plasma wave-induced cross-focusing and guiding

3.1. Bi-envelope equations

As in any PBWA, the entering beam (1) is bi-color. The tendency to focus/de-focus can be well captured by the bi-envelope model which includes only the modes $l = 0, 1$ and neglects the effect of GVD. Limitations of this assumption are discussed later in section 3.3. The set

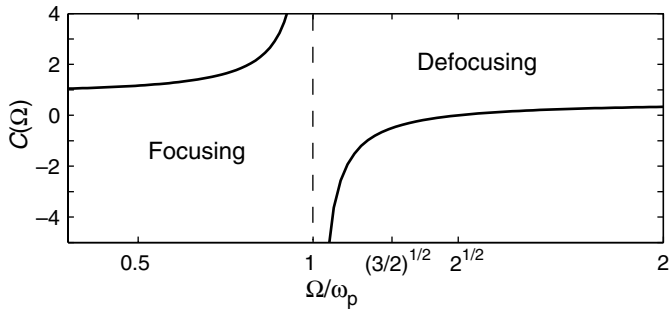

Figure 1. Cross-focusing coefficient C given by equation (6*c*) as a function of normalized beat frequency.

of coupled paraxial equation (4) reduces to

$$(2\mathrm{i}k_l\partial/\partial z + \Delta_\perp)a_l \approx k_l^2(1-\eta_l^2)a_l, \tag{6a}$$

$$1-\eta_l^2 = -(k_\mathrm{p}/2k_l)^2(|a_l|^2 + 2C|a_m|^2), \tag{6b}$$

$$C = 1 - C_\mathrm{N} \equiv 1 - (\tilde{\Omega}^2/2)/(\tilde{\Omega}^2 - 1), \tag{6c}$$

where the subscripts are $(l, m) = (0, 1)$ and $(1, 0)$, and $\tilde{\Omega} = \Omega/\omega_\mathrm{p}$ is the normalized beat frequency. The first term in (6*b*) describes the relativistic *self-focusing* of each beam, and the second—the nonlinear *cross-focusing*. Their relative magnitude and sign determine whether the nonlinear correction to the index leads to the focusing or de-focusing. The first term in the cross-focusing coefficient (6*c*) results from the relativistic mass effect [13]. The second term, $C_\mathrm{N} \equiv N_1/(a_0^* a_1)$, is responsible for the plasma wave-induced cross-focusing. Its sign is determined by the magnitude of the beat frequency $\tilde{\Omega}$. The cross-focusing coefficient $C(\tilde{\Omega})$ is plotted in figure 1. In the most interesting case of $\tilde{\Omega} \approx 1$, it is determined almost entirely by the plasma wave contribution: $C \approx [4(1-\tilde{\Omega})]^{-1}$. In this case the nonlinear focusing is enhanced if $\tilde{\Omega} < 1$, while the de-focusing is induced for $\tilde{\Omega} > 1$.

From the coupled partial differential equation (6*a*), we derive a set of coupled ordinary differential equations for the spot size evolution using the SDE. SDE is a universal technique originally applied to free-electron lasers [33], and later to laser–plasma [10, 13, 17], and electron beam–plasma [38] interactions. Neglecting the aberrations (higher-order Laguerre–Gaussian modes), we approximate each beam with the lowest order Gaussian mode, $a_l = A_l \exp[\mathrm{i}(\theta_l + \alpha_l r^2/r_l^2) - r^2/r_l^2]$, completely defined by the four real-valued parameters: amplitude $A_l(z, \xi)$, spot size $r_l(z, \xi)$, Gouy phase shift $\theta_l(z, \xi)$, and normalized inverse curvature of wavefront $\alpha_l(z, \xi)$. Dependence on ξ is purely parametrical (i.e. the beam slices taken at different ξ evolve independently), which is a consequence of the local plasma response (3). These parameters satisfy the evolution equations [33]

$$\partial(A_l r_l)/\partial z = (A_l r_l)\mathrm{Im}\, G_l, \tag{7a}$$

$$\partial\theta_l/\partial z = -2/(k_l r_l^2) - \mathrm{Re}(G_l + H_l), \tag{7b}$$

$$\partial\alpha_l/\partial z = 2(1+\alpha_l^2)/(k_l r_l^2) + 2(\mathrm{Re}\, H_l - \alpha_l\, \mathrm{Im}\, H_l), \tag{7c}$$

$$\partial r_l/\partial z = 2\alpha_l/(k_l r_l) - r_l\, \mathrm{Im}\, H_l. \tag{7d}$$

The right-hand sides of these equations contain the nonlinear source moments [33] $G_l = (k_l/2)\int_0^\infty (1-n_l^2)\exp(-\chi_l)\,\mathrm{d}\chi_l$, $H_l = k_l\int_0^\infty \chi_l(\partial n_l/\partial\chi_l)\exp(-\chi_l)\,\mathrm{d}\chi_l$, where $\chi_l = 2r^2/r_l^2$.

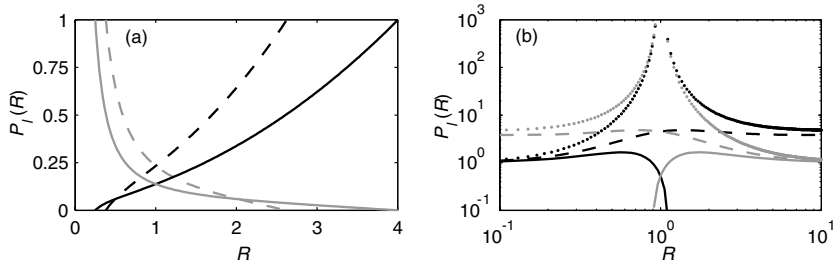

Figure 2. Normalized power for matched solutions P_0 (black) and P_1 (gray) plotted as a function of area ratio $R = (r_{00}/r_{01})^2$ for different detunings (*a*) $\tilde{\Omega} < 1$ [$\tilde{\Omega} = 0.75$ (dashed), $\tilde{\Omega} = 0.9$ (solid)], (*b*) $\tilde{\Omega} > 1$ [$\tilde{\Omega} = \sqrt{3/2}$ (dots), $\tilde{\Omega} = 1.25$ (dashed), $\tilde{\Omega} = 3.18$ (solid)].

A straightforward calculation shows that these moments are real-valued:

$$G_l = -(k_p^2/16k_l)[A_l^2 + 4C A_m^2 r_m^2/(r_m^2 + r_l^2)], \tag{8a}$$

$$H_l = -(k_p^2/32k_l)[A_l^2 + 8C A_m^2 r_m^2 r_l^2/(r_m^2 + r_l^2)^2]. \tag{8b}$$

The inclusion of additional laser sidebands makes G_l and H_l complex valued. With the real source moments, power of an individual beam in a given ξ-slice is preserved. Hence, from equation (7*a*), $A_l(z, \xi) = A_{0l}(\xi) r_{0l}/r_l(z, \xi)$, where $A_{0l}(\xi)$ and r_{0l} are initial amplitude and spot size of the lth component. Equation (7*d*) expresses the inverse wavefront curvature through the spot size, $\alpha_l(z, \xi) = (k_l/4)\partial r_l^2/\partial z$. Differentiating equation (7*d*) over z and using (7*c*) gives the coupled equations for the spot sizes

$$\partial^2 r_l/\partial z^2 = (4/k_l^2 r_l^3)[1 - P_l - 8C P_m r_l^4/(r_m^2 + r_l^2)^2], \tag{9}$$

where $P_l(\xi) = A_{0l}^2(\xi)(k_p r_{0l})^2/32$ is the instant power of lth beam normalized to the critical power of a monochromatic beam. We assume that the beams with different amplitudes and spot sizes are focused at $z = 0$ and overlap in time. Hence, the initial conditions are $r_l(z = 0) = r_{0l}$ and $\partial r_l/\partial z(z = 0) = 0$. Solving the initial value problem for equation (9) and calculating the complex envelopes a_l, we can reconstruct the entire bi-color beam at a distance $z > 0$ by using equation (2).

3.2. Matched propagation of the beams and all-optical suppression of RSF

The stationary points of equation (9) correspond to the matched propagation (mutual guiding) of the beams. The condition for matched propagation gives the normalized instant powers P_l in terms of the cross-focusing coefficient C and the area ratio $R = (r_{00}/r_{01})^2$:

$$P_l = (1 + R)^2[(1 + R)^2 - 8C R^{2m}][(1 + R)^4 - 64C^2 R^2]^{-1}. \tag{10}$$

Without plasma wave ($C = 1$), these expressions reduce to those earlier obtained by Esarey *et al* [13]. Representative solutions (10) are displayed in figure 2. One can check that the higher-power beam confines the lower-power one with a smaller radius. The matched equal-area ($R = 1$) beams have the same power:

$$P_0 = P_1 \equiv P_{eq} = (1 + 2C)^{-1} = (1 - \tilde{\Omega}^2)/(3 - 2\tilde{\Omega}^2). \tag{11}$$

The plasma wave-induced focusing threshold analytically found earlier for equal-area beams with $\Omega - \omega_p = -3\omega_{RL}$ (equation (28) of paper [14]) is a special case of (11).

The requirement of $P_l > 0$ limits the range of possible C and R. In the case $\tilde{\Omega} < 1$ (then $C > 1$), the equilibria of two unequal beams can exist in the range

$$(\sqrt{8C} - 1)^{-1} < R < \sqrt{8C} - 1, \tag{12}$$

and mutual guiding requires less power than the self-guiding of a monochromatic beam: $P_0 + P_1 < 1$. As $\tilde{\Omega} \to 1$ (then $C \to \infty$), the interval (12) extends infinitely, hence two beams with virtually any area ratio can be matched with the appropriate choice of power partition. In this regime, the nonlinear focusing is determined mostly by the plasma wave (the effect earlier dubbed the 'cascade focusing' [14]): for $\tilde{\Omega} = 0.9$ and $R = 1$ equation (11) gives $P_{\rm eq} \approx 0.138$, which is less than one-half of that given by the relativistic mass effect only: $P_{\rm eq}(C = 1) = \frac{1}{3}$ [12, 13].

In the case $\tilde{\Omega} > 1$ (then $C < \frac{1}{2}$), the matched solutions exist if $0 < R < R_-$ or $R > R_+$, where $R_\pm = 4|C| - 1 \pm [(4|C| - 1)^2 - 1]^{1/2}$. Generally, as is seen in figure 2(*b*), de-focusing effect of the plasma wave increases the total power of the matched beams above the critical power for a monochromatic beam ($P_0 + P_1 > 1$). In the regime with moderate over-detuning ($1 < \tilde{\Omega} < \sqrt{2}$, $C < 0$), the plasma wave-induced de-focusing overcomes the net effect of RSF and RCF; matching the beams with similar parameters ($P_0 \sim P_1$, $R \sim 1$) becomes either impossible (if $1 < \tilde{\Omega} \leqslant \sqrt{3/2}$) or requires over-critical power for each beam (if $\sqrt{3/2} < \tilde{\Omega} < \sqrt{2}$). Finally, in the strongly over-detuned regime ($\tilde{\Omega} \to \infty$, $C \to \frac{1}{2}$) only equal-area pulses can be matched. In this limit, equation (9) gives the mutual guiding condition $P_0 + P_1 = 1$, which depends on the total energy, and not on the power partition.

Enhanced mutual de-focusing of the two beams in the regime with moderate over-detuning ($1 < \tilde{\Omega} < \sqrt{2}$) can be utilized in practice to prevent the catastrophic RSF of an over-critical monochromatic beam. Splitting a small fraction of the beam energy into the frequency-shifted sideband with the same spot size can turn the catastrophic RSF into a mild de-focusing of the bi-color beam. To this effect, the normalized power of the split beam must exceed the threshold

$$P_1 \geqslant (P_{\rm tot} - 1)(\tilde{\Omega}^2 - 1), \tag{13}$$

where $P_{\rm tot} = P_0 + P_1 > 1$ is the normalized power of the original beam (the beam '0' may still be over-critical, $P_0 > 1$). To visualize the effect of beam splitting on the nonlinear focusing we employ the mean-square radius $\langle r^2 \rangle$ defined in section 2. Flux conservation for the individual frequency components yields

$$\langle r^2(z) \rangle = \frac{\sum_l k_l (A_l r_l)^2 r_l^2}{2 \sum_l k_l (A_l r_l)^2} = \frac{k_0 P_0 r_0^2(z) + k_1 P_1 r_1^2(z)}{2(k_0 P_0 + k_1 P_1)}, \tag{14}$$

For numerical demonstration, we choose $\tilde{\Omega} = 1.25$, $R = 1$, $\omega_{\rm p}/\omega_0 = 0.018$, $P_{\rm tot} = 1.1$, and use the solution of equation (9) to track the evolution of spot sizes r_l and $\langle r^2 \rangle$ over $Z_{\rm R}/2$ (where $Z_{\rm R} = k_0 r_{00}^2/2$ is the Rayleigh length). The results are plotted in figure 3. Equation (13) becomes an equality for the power partition $P_1/P_0 = 0.054$ ($P_0 = 1.043\,75$ and $P_1 = 0.056\,25$), in which case the spot of the higher-power (still over-critical) beam remains nearly constant. The weak beam quickly diffracts, hence the mean-square radius slowly grows (i.e. the entire bi-color beam mildly diffracts). For larger power partition (see the graphical example for $P_1/P_0 = \frac{3}{17}$) spot sizes grow for both beams thereby enhancing the whole-beam diffraction.

3.3. All-optical suppression of nonlinear focusing: numerical analysis

In this section we examine how the initial suppression of the RSF affects the laser beam dynamics over a large propagation distance. Simplified analysis based on the bi-envelope model is only capable of capturing the initial tendency of beams to de-focus. Bi-envelope theory without aberrations describes the ground state from which both electromagnetic cascade [14, 26, 30–32] and the Raman-type instabilities [2, 10, 22–25, 39] grow. Stationary and non-stationary filamentation can also manifest [40] if the over-critical beam propagates over a few

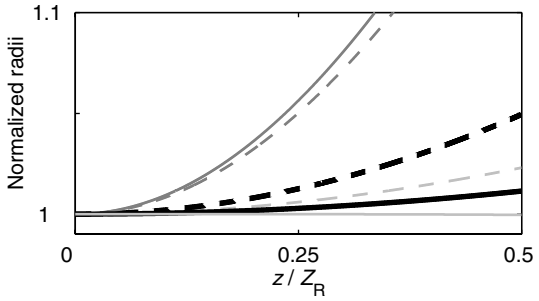

Figure 3. Evolution of the normalized spots r_0/r_{00} (light gray), r_1/r_{00} (dark gray), and mean-square radius $\langle r^2/r_{00}^2\rangle^{1/2}$ (black) for the bi-color beam with over-critical total power ($P_{\rm tot} = 1.1$) and difference frequency $\tilde{\Omega} = 1.25$. The beam components have initially the same area ($R = 1$); power partition is $P_1/P_0 = 0.054$ (solid) and $P_1/P_0 = \frac{3}{17}$ (dashed).

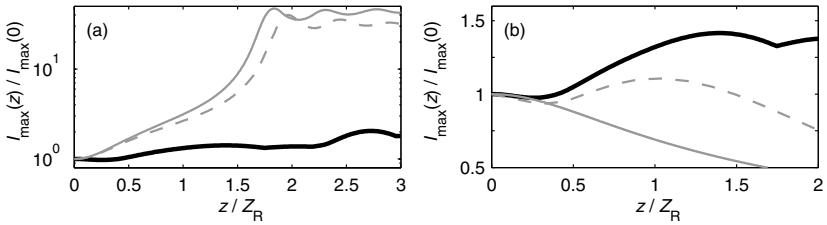

Figure 4. Laser peak intensity versus propagation distance. Physical parameters are specified in the text. Plot (*a*) shows the results of WAKE simulation results for the monochromatic (solid gray) and bi-color, $\tilde{\Omega} = 3.18$ (dashed gray), $\tilde{\Omega} = 1.25$ (black), laser pulse. Plot (*b*) compares the WAKE result (black curve from the plot (*a*)) with the results of bi-color model (solid gray) and the cascade simulation with local electron response (dashed gray).

Rayleigh lengths. Therefore, we have to assess the long-term dynamics of initially bi-color system using fully nonlinear simulations with the dynamic plasma response.

Our main tool is the 3D axi-symmetric (in cylindrical geometry) fully relativistic PIC code WAKE [9]. It solves for the envelope of linearly polarized laser beam in the extended paraxial approximation (GVD included). The plasma response to the time-averaged (over laser period) ponderomotive force is quasi-static. The laser beam propagates through the plasma in the positive z direction. Simulation starts at the vacuum focal plane $z = 0$ with the boundary condition for radiation (1), where $a_l(r, 0, \xi) = A_{0l}\exp[-r^2/r_{0l}^2 - 2\ln 2\xi^2/(c\tau_{\rm L})^2]$. Plasma is uniform and quiescent ahead of the laser ($\xi \to -\infty$). For the simulation, we borrow one set of parameters from figure 3. An over-critical bi-color beam ($P_{\rm tot} = 1.1$, $\tilde{\Omega} = 1.25$, $R = 1$) propagates numerically from $z = 0$ to $z = 3Z_{\rm R}$ in a plasma with $\omega_{\rm p}/\omega_0 = 0.018$. The beam duration and spot size are $\tau_{\rm L} \approx 55\omega_{\rm p}^{-1}$ and $r_{0l} = 16.5k_{\rm p}^{-1}$ (hence $A_{00}^2 + A_{01}^2 \approx 0.13$). For the laser with a fundamental wavelength $\lambda_0 = 0.8\,\mu$m this corresponds to $\tau_{\rm L} \approx 1.3$ ps, 55 TW total power, and plasma length 16 cm. In order to concentrate on the whole-beam effects (diffraction, self-focusing, RMI) we choose rather coarse transverse grid, $\Delta r = r_{00}/22$, with 20 particles per radial cell.

When the pulse is initially monochromatic ($A_{01} = 0$), its central (over-critical) part almost collapses due to the catastrophic RSF. Figure 4(*a*) (solid gray curve) shows the enhancement of peak intensity by a factor ~50. The collapse stabilizes around $z \approx 2Z_{\rm R}$ through the formation of an evacuated electron density channel, $n(r = 0) < 0.1n_0$ (not shown). The tightly focused

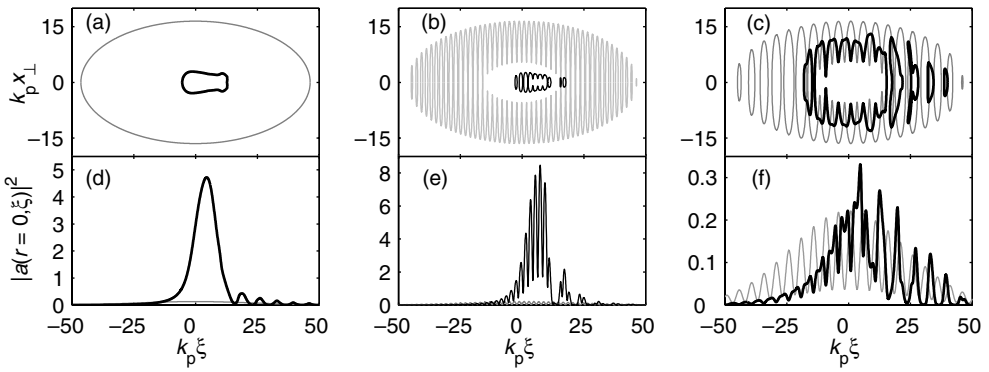

Figure 5. Laser intensity profiles from the WAKE simulations of figure 4(*a*) at $z = 0$ (gray) and $z = 2Z_R$ (black). Top: iso-contours of laser intensity at the level e^{-2} of the maximum (only the central part of actual simulation box is shown). Bottom: axial lineouts of normalized intensity. Left column—initially monochromatic pulse with $P_0 = 1.1$; middle column—bi-color pulse with power partition $P_1/P_0 = 3/17$, $P_0 + P_1 = 1.1$, $\tilde{\Omega} = 3.18$; right column—bi-color pulse with the same power partition and $\tilde{\Omega} = 1.25$.

pulse (figures 5(*a*) and (*d*)) is further guided by the channel. Dynamics of initially bi-color beam ($P_1/P_0 = \frac{3}{17}$) with a large difference frequency ($\tilde{\Omega} = 3.18$) follows exactly the same scenario (dashed gray curve in figure 4(*a*) and intensity profiles in figures 5(*b*) and (*e*)). Therefore, as we have found in section 3.2, splitting the beam into a pair of far off-resonant components ($\Omega \gg \omega_p$) does not help suppress the RSF.

Conversely, as Ω approaches ω_p (we provide here an example for $\tilde{\Omega} = 1.25$ and $P_1/P_0 = \frac{3}{17}$), the laser beam shows no tendency to collapse. Instead, it propagates over three Rayleigh lengths with the steadily varying peak intensity and spot size (black curves in figures 4(*a*) and (*b*) and intensity profiles in figures 5(*c*) and (*f*)). In the very beginning, fully dynamic WAKE simulation perfectly agrees with the semi-analytic bi-envelope model (solid gray curve in figure 4(*b*)). The modest electron density perturbation, $N_1 \approx 0.06$, totally suppresses the relativistic mass effects, and the peak laser initially drops. For $z > Z_R/4$ this agreement is violated. This is *not* the deficiency of the local plasma response approximation and is rather a consequence of electromagnetic cascading. Indeed, the cascading is negligible over the distance $z < Z_R(P_0P_1)^{-1/2}(\tilde{\Omega}^2 - 1)/(4\tilde{\Omega}^2) \approx Z_R/4$ [30]. As we solve numerically the full electromagnetic cascade model (4) and allow the sidebands to grow on each side of the fundamental, much better agreement with the WAKE simulation is achieved (compare gray dashed and black curves in figure 4(*b*)). In both simulations, three satellites on each side of ω_0 are produced around $z \approx Z_R$ (laser spectrum from the WAKE simulation can be seen in figure 6(*a*)). In addition, we find from the cascade modelling (4) that each individual beam (especially the near-critical one) becomes transversely non-Gaussian within a fraction of a Rayleigh length. The electromagnetic cascading thus reverses the tendency to de-focus, but without collapse.

Spectral analysis reveals another cause for the enhancement of focusing. By analogy with equations (3) and (6*c*) we define the plasma wave-induced cross-focusing coefficient in the frequency domain, $C_N^\Omega = N_e(\Omega)/(a^*(\omega_0)a(\omega_0 - \Omega))$, where $N_e(\omega)$ and $a(\omega)$ are Fourier transforms of the density perturbation and laser envelope (figures 6(*a*) and (*b*)), and track its evolution along the laser path (figure 6(*c*)). C_N^Ω is constant in the bi-envelope model; hence, the de-focusing persists over the entire propagation distance. In contrast, $|C_N^\Omega|$ gradually decays in the fully dynamic simulation, and the de-focusing turns into a mild focusing.

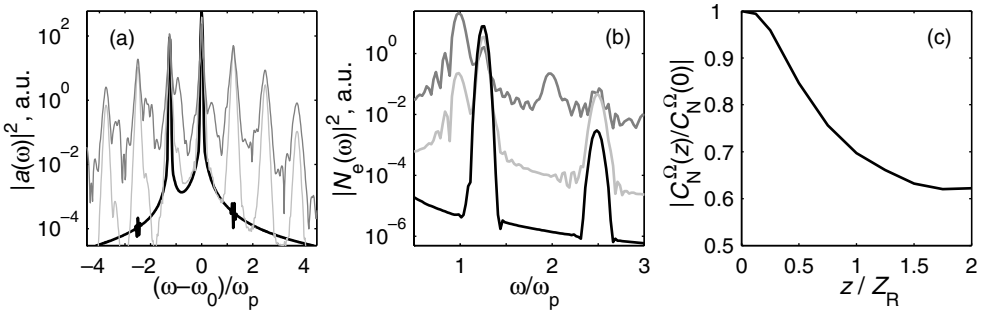

Figure 6. Spectral evolution of (*a*) laser radiation and (*b*) plasma density perturbations from the simulation of figures 5(*c*) and (*f*). Radially integrated spectra are shown for $z = 0$ (black), $z = Z_R$ (light gray), $z = 2Z_R$ (dark gray). Plot (c): plasma wave-induced cross-focusing coefficient versus propagation distance.

The later stage of propagation ($z \geqslant 1.5Z_R$) is dominated by the spontaneous RMI [10] and near-forward SRS [25, 39]. Indeed, laser spectra in figure 6(*a*) include weak Raman features shifted by integer multiples of ω_p. Besides, figure 6(*b*) shows that the non-resonant density perturbations $N_e(\omega = \Omega)$ gradually decay, while the resonant plasma response $N_e(\omega = \omega_p)$ (responsible for the RMI and SRS) becomes dominant. Erosion of the beam tail due to the SRS is clearly seen in the laser intensity profiles in figures 5(*c*) and (*f*). The total laser energy depletion is, however, very low ($< 5\%$).

4. Accelerator applications

4.1. Over-detuned beat wave

Injected electrons can be effectively accelerated in the PBWA with suppressed self-focusing ($P_0 \geqslant 1$, $P_1/P_0 \ll 1$, $\tilde{\Omega} > 1$). Remarkable laser stability over centimetre-long plasmas without external guiding, the electron energy gain in excess of 100 MeV, and the electron beam quality competitive with the existing plasma-based accelerator schemes make the over-detuned PBWA practically interesting.

In the simulation of figures 5(*c*) and (*f*), the accelerating gradient E_{acc} is about 5% of the 1D cold wavebreaking limit, $E_{br} = cm_e\omega_p/|e|$ [41] (in practical units, $E_{acc} \sim 4\,\mathrm{GV\,m^{-1}}$). In this run, a long, monoenergetic ($\gamma_{e0} = 15$), longitudinally uniform bunch of test electrons (beam loading neglected) is injected with a zero angular spread around the peak of accelerating gradient in the focal plane ($z = 0$). The bunch density is axi-symmetric Gaussian with the root-mean-square size $\sigma = 5k_p^{-1} \approx 35\,\mu$m, Such beams are typical of state-of-art RF guns [35]. The low energy at injection, $\gamma_{e0} < \omega_0/\omega_p$, is chosen in order to reduce the final energy spread [29, 42–44]. The particle tracking procedure in the code WAKE is fully 3D and includes direct interaction of electrons with the high-frequency laser field [45].

The acceleration proceeds in a quasi-monoenergetic fashion until $z \approx Z_R$. Beyond that point the energy distribution broadens. Laser erosion due to the growing near-forward SRS destroys the coherence of accelerating-focusing fields, and acceleration becomes inefficient. Typical energy spectra are shown in figure 7(*a*). At $z = 0.9Z_R \approx 4.8$ cm, the energy spectrum is centred at $\gamma = 200$ with 30% full width at half-maximum. The normalized transverse emittance $\gamma\varepsilon_\perp \approx 2.5\pi$ mm mrad is preserved over the entire acceleration distance. Because electrons are injected into six EPW buckets, figure 7(*b*) shows six clearly distinguishable

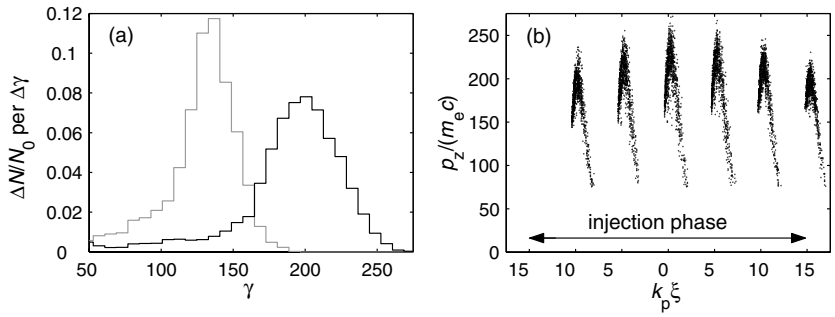

Figure 7. (*a*) Energy spectrum of test electrons crossing the planes $z = 0.5Z_R$ (gray) and $z = 0.9Z_R$ (black), $Z_R \approx 5.3$ cm. Number of accelerated electrons per energy spectrometer bin is shown (the bin size $\Delta\gamma = 8$). (*b*) Longitudinal phase space of particles with $\gamma > 75$ at $z = 0.9Z_R$. $N_0 = 9000$ electrons with $\gamma_{e0} = 15$ were injected in 6 consecutive beat wave periods around the peak of accelerating gradient ($-15 < k_p\xi_{inj} < 15$, as indicated in plot (*b*)).

accelerated bunches separated in time by $2\pi/\Omega \approx 120$ fs. The maximum charge that each bunch can carry without increasing the energy spread is determined by the beam loading threshold [46]. For this simulation, the limit is 6.5 pC per bucket (total $\sim$ 40 pC in six buckets).

4.2. Under-detuned beat wave

In the under-detuned regime ($\Omega < \omega_p$), even under-critical beams ($P_l \ll 1$) can be strongly focused by the driven EPW. Focusing dynamics, however, is non-stationary and strongly depends on the laser pulse shape and duration [26, 27]. The driven EPW acts as the periodic focusing channel. Focusing the laser beat notes, in turn, enhances the electron density perturbation. The feedback loop persists until the EPW becomes very nonlinear. This is exactly the scenario of seeded RMI [20, 21]. Parameter scalings for this regime and examples of electron acceleration can be found in [27].

As the assumption of local plasma response fails from the very beginning, we resort to the fully dynamic WAKE simulations. For the numerical demonstration, we take two identical beams separated in frequency by $\tilde{\Omega} = 0.9$. Other laser and plasma parameters are $\lambda_0 = 0.8\,\mu$m, $\omega_p/\omega_0 \approx 10^{-3/2}$, $\tau_L \approx 50\omega_p^{-1}$ and $r_{00} = 14.14k_p^{-1}$ [26]. The normalized peak power of each beam, $P_l \approx 0.14$ (2.25 TW in physical units), satisfies the condition of matched propagation (11) from the bi-envelope theory. The numerical experiment, however, shows dramatic enhancement of the beam focusing and the EPW growth almost to the point of transverse wave breaking [47]. Figure 8(*a*) shows saturation of the nonlinear focusing around $z = 0.65Z_R$. Stimulated Raman cascade significantly broadens the laser frequency spectrum (displayed in figure 8(*b*)). Broad bandwidth laser beat notes are further guided by the 3D plasma wave buckets [10, 16, 48] and compressed temporally by the GVD. The entire beam is finally transformed into the train of intense few-cycle spikes [26, 27]. Figure 8(*c*) shows that the driven EPW changes very steadily from $z = Z_R$ to $z = 2Z_R$. It maintains an average accelerating gradient $E_{acc} \approx 30$ GeV m^{-1}. The electron density buckets cannot totally confine the ultrashort laser spikes, and the EPW decays after $Z = 2Z_R$.

Unstable behavior of the EPW over the initial stage of propagation requires electron injection inside the plasma slab (possibly, by using the head-on colliding laser beams [36]). The test particle simulation shows that the electrons injected at $z = Z_R$ with $\gamma_{e0} = 1.5$ gain

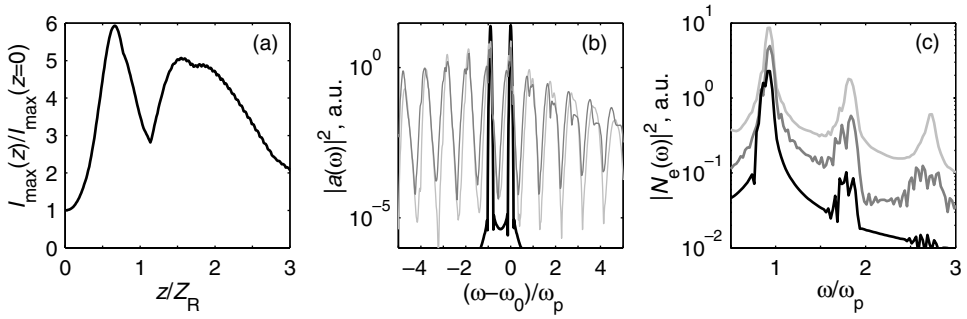

Figure 8. (*a*) Laser peak intensity as a function of propagation distance. Spectral evolution of (*b*) laser radiation and (*c*) plasma density perturbations. Radially integrated spectra are shown for $z = 0$ (black), $z = Z_R$ (light gray), $z = 2Z_R$ (dark gray). Two identical laser beams with the difference frequency $\tilde{\Omega} = 0.9$ and normalized power $P_l = 0.14$ were injected into plasma at $z = 0$.

about 350 MeV at the extraction point $z = 2Z_R$ (acceleration length 1.3 cm) with the energy spread below 10%. The beam loading limits the charge per bucket to <20 pC.

5. Conclusion

We have demonstrated that the nonlinear focusing of a bi-color laser beam in tenuous plasmas can be all-optically enhanced or suppressed depending whether the beat wave frequency Ω is below or above the electron Langmuir frequency ω_p. Self-consistent guiding of a mildly over-critical ($P > P_{cr}$) long ($\omega_p\tau_L \gg 1$) laser beam can be all-optically initiated by optical mixing with a second, much weaker, beam shifted in frequency by $\Omega > \omega_p$. The guiding effect initially owes to the de-focusing properties of the laser beat wave-driven 3D electron density perturbation. Electromagnetic cascading and resonant self-modulation contribute to the guiding process at propagation distances over one Rayleigh length. Practical implementation of this guiding scheme calls for the bi-color laser light sources, one example of which has been recently reported in literature [49]. The over-detuned ($\Omega > \omega_p$) PBWA can accelerate quasi-monoenergetic bunched electron beams beyond a hundred MeV energy. In the case of $\Omega < \omega_p$, acceleration efficiency is generally higher because of nonlinear focusing enhanced by the plasma wave excitation. In this regime, however, initial evolution of the plasma wave precludes quasi-monoenergetic acceleration of externally injected electrons, hence the electrons should be injected in the plasma wake at a considerable distance from the plasma boundary. This technical difficulty can be, possibly, bypassed with the all-optical injection technique using the head-on colliding laser beams [36].

Acknowledgments

This work is supported by the US DoE Grants DE-FG02-04ER54763, DE-FG02-04ER41321, DE-FG02-07ER54945, and by the NSF Grant PHY-0114336 administered by the FOCUS Center at the University of Michigan, Ann Arbor.

References

[1] Tajima T and Dawson J M 1979 *Phys. Rev. Lett* **43** 267–70
[2] Esarey E, Sprangle P, Krall J and Ting A 1996 *IEEE Trans. Plasma Sci.* **PS-24** 252–88
[3] Andreev N E and Kuznetsov S V 2003 *Plasma Phys. Control. Fusion* **45** A39–57

[4] Malka V, Faure J, Glinec Y and Lifschitz A F 2005 *Plasma Phys. Control. Fusion* **47** B481—90
[5] Litvak A G 1970 *Sov. Phys.—JETP* **30** 344
[6] Max C, Arons J and Langdon B 1974 *Phys. Rev. Lett.* **33** 209–12
[7] Sun G Z, Ott E, Lee Y C and Guzdar P 1987 *Phys. Fluids* **30** 526–32
[8] Shen Y R 1984 *The Principles of Nonlinear Optics* (New York: Wiley)
[9] Mora P and Antonsen T M 1997 *Phys. Plasmas* **4** 217–29
[10] Esarey E, Sprangle P, Krall J and Ting A 1997 *IEEE J. Quantum Electron.* **QE-33** 1879–914
[11] Hafizi B, Ting A, Sprangle P and Hubbard R F 2000 *Phys. Rev.* E **62** 4120–5
[12] Litvak A G and Fraiman G M 1972 *Radiophys. Quantum Electron.* **15** 1024–9
[13] Esarey E, Ting A and Sprangle P 1988 *Appl. Phys. Lett.* **53** 1266–8
[14] Gibbon P 1990 *Phys. Fluids* B **2** 2196–208
[15] Gibbon P and Bell A R 1988 *Phys. Rev. Lett.* **61** 1599–602
Gibbon P and Bell A R 1988 *Phys. Rev. Lett.* **61** 2509
[16] Esarey E and Ting A 1990 *Phys. Rev. Lett.* **65** 1961
Gibbon P and Bell A R 1990 *Phys. Rev. Lett.* **65** 1962
[17] Shvets G and Pukhov A 1999 *Phys. Rev.* E **59** 1033–7
[18] Joshi C, Clayton C E and Chen F 1982 *Phys. Rev. Lett.* **48** 874–7
[19] Mori W B *et al* 1988 *Phys. Rev. Lett.* **60** 1298–301
[20] Andreev N E, Kirsanov V I and Gorbunov L M 1995 *Phys. Plasmas* **2** 2573–82
[21] Fomyts'kyi M, Chiu C, Downer M and Grigsby F 2005 *Phys. Plasmas* **12** 023103
[22] Andreev N E *et al* 1992 *JETP Lett.* **55** 571–4
[23] Sprangle P, Esarey E, Krall J and Joyce C 1992 *Phys. Rev. Lett.* **69** 2200–3
[24] Antonsen T M and Mora P 1992 *Phys. Rev. Lett.* **69** 2204–7
[25] Antonsen T M and P. Mora 1993 *Phys. Fluids* B **5** 1440–52
[26] Kalmykov S and Shvets G 2006 *Phys. Plasmas* **13** 056707
[27] Kalmykov S and Shvets G 2006 *AIP Proc.* **877** 395–401
[28] Sprangle P, Esarey E and Ting A 1990 *Phys. Rev.* A **41** 4463–9
[29] Gorbunov L M, Kalmykov S Y and Mora P 2005 *Phys. Plasmas* **12** 033101
[30] Kalmykov S and Shvets G 2006 *Phys. Rev.* E **73** 046403 (arXiv:physics/0511195)
[31] Cohen B I, Kaufman A N and Watson K M 1972 *Phys. Rev. Lett.* **29** 581–4
[32] Kalmykov S and Shvets G 2005 *Phys. Rev. Lett.* **94** 235001
[33] Sprangle P, Ting A and Tang C M 1987 *Phys. Rev.* A **36** 2773–81
[34] Filip C V *et al* 2004 *Phys. Rev.* E **69** 026404
[35] de Loos M J *et al* 2006 *Phys. Rev. ST Accel. Beams* **9** 084201
[36] Faure J, Rechatin C, Norlin A, Lifschitz A, Glinec Y and Malka V 2006 *Nature* **444** 737–9
[37] Rosenbluth M N and Liu C S 1972 *Phys. Rev. Lett.* **29** 701–5
[38] Govil R, Leemans W P, Backhaus E Y and Wurtele J S 1999 *Phys. Rev. Lett.* **83** 3202–5
[39] Tzeng K C and Mori W B 1998 *Phys. Rev. Lett.* **81** 104–7
[40] Andreev N E, Gorbunov L M, Mora P and Ramazashvili R R 2007 *Phys. Plasmas* **14** 083104
[41] Dawson J M 1959 *Phys. Rev.* **113** 383–7
[42] Gordon D F *et al* 2005 *Phys. Rev.* E **71** 026404
[43] Lifschitz A F, Faure J, Malka V and Mora P 2005 *Phys. Plasmas* **12** 093104
[44] Kalmykov S Y, Gorbunov L M, Mora P and Shvets G 2006 *Phys. Plasmas* **13** 113102
[45] Malka V *et al* 2001 *Phys. Plasmas* 2605–8
[46] Khachatryan A G *et al* 2004 *Phys. Rev. ST Accel. Beams* **7** 121301
[47] Bulanov S V, Pegoraro F, Pukhov A M and Sakharov A S 1997 *Phys. Rev. Lett.* **78** 4205–8
[48] Bulanov S V and Sakharov A S 1991 *JETP Lett.* **54** 203–6
[49] Grigsby F, Peng Dong and Downer M 2008 *J. Opt. Soc. Am.* B **25** 346–50